JOURNAL OF Materials CHEMISTRY

The manganese nitrides η-Mn_3N_2 and θ-Mn_6N_{5+x}: nuclear and magnetic structures

Andreas Leineweber,[a]† Rainer Niewa,[b] Herbert Jacobs*[a] and Winfried Kockelmann[c,d]

[a]*Lehrstuhl AC I, Fachbereich Chemie der Universität, 44221 Dortmund, Germany. E-mail: jacobs@pop.uni-dortmund.de*
[b]*Max-Planck-Institut für Chemische Physik fester Stoffe, 01187 Dresden, Germany*
[c]*ISIS, Rutherford Appleton Laboratory, Chilton, UK OX11 0QX*
[d]*Mineralogisch-Petrologisches Institut, Universität Bonn, 53115 Bonn, Germany*

Received 29th August 2000, Accepted 31st August 2000
First published as an Advance Article on the web 26th October 2000

Neutron powder diffraction measurements on η-Mn_3N_2 and θ-Mn_6N_{5+x} ($x=0.26$) revealed the nuclear and magnetic structures of these metallic interstitial compounds.

At ambient temperatures the crystal structures of both materials derive from an fcc arrangement of Mn with N occupying octahedral sites. The unit cells are face-centred tetragonal, η-Mn_3N_2: $a=4.2046(1)$ Å, $c=12.131(1)$ Å $\approx 3\times 4.041$ Å; θ-$Mn_6N_{5.26}$: $a=4.2193(1)$ Å, $c=4.1287(1)$ Å. Both phases show an antiferromagnetic ordering of the first kind with magnetic moments between 3.3 and 3.8 μ_B.

The data for η-Mn_3N_2 confirm a previously reported ordered arrangement of N on 2/3 of the octahedral sites and the collinear antiferromagnetic superstructure with the magnetic moments oriented perpendicular to the tetragonal c axis. However, a close inspection of the data reveals some systematic ambiguities of the magnetic structure which are analysed in detail.

In θ-Mn_6N_{5+x} ($x=0.26$) the N atoms show no long-range occupational order on the octahedral sites. At ambient temperatures the collinear magnetic moments are tilted by 23° relative to the tetragonal c axis. High temperature neutron powder diffraction measurements reveal a simultaneous decay of the sublattice magnetisations and the tetragonal distortion of the cell dimensions. At about 550 K the magnetic moments align parallel to the c axis, and up to the critical temperature of 660 K they decrease continuously to zero. Parallel to this, the tetragonal distortion of the unit cell reduces and finally approaches a face-centred cubic structure.

The consequences of the results with respect to the Mn/N phase diagram are discussed.

Most of the binary nitrides MN_y with M = 3d metal and $y<1$ may be classified as interstitial nitrides.[1] These are, in general, harder, less ductile and less sensitive towards corrosion than the parent metals. From these properties the technological importance[2] of 3d metal nitrides is derived. In particular, iron nitrides are often generated on the surfaces of work pieces made of steel. Also nitrides of many alloy elements are formed during such processes, including manganese nitrides.[2]

The crystal structures of interstitial nitrides in most cases derive from an fcc or hcp arrangement of M with N occupying octahedral sites in a more or less ordered way.[1,3] Most studies on the crystal structures of interstitial nitrides are based on X-ray diffraction on powders. Owing to the small scattering power of N compared to that of the metal atoms, this method allows only a qualitative investigation of the superstructures caused by ordering of N. However, neutron diffraction[4] is a powerful tool to study quantitatively ordered distributions of N in interstitial nitrides of 3d metals.[5–11] The nuclear scattering length of N is one of the highest of all elements of the Periodic Table. Furthermore, neutron diffraction can give valuable information about long-range ordered magnetic structures occurring in many nitrides of 3d metals[7–9,12–15] which are of particular theoretical interest in comparison to the magnetic properties of the pure 3d metals.

For $y>0.5$ two different manganese nitride phases MnN_y are reported (for a review see ref. 16): the η-phase ($0.61<y<0.69$) and the θ-phase ($0.85<y<0.96$). The crystal structures of both phases are based on a tetragonally distorted fcc arrangement of Mn with $c/a<1$ (relative to the fcc unit cell) with N on slightly distorted octahedral interstices. Whereas manganese nitrides with $y<0.5$ can readily be prepared from Mn and N_2, for the synthesis of nitrides with $y>0.5$ commonly NH_3 or NH_3/H_2 is passed over Mn. In many cases this method is used to prepare nitrides which cannot be obtained from metal and nitrogen with attainable pressures.[17,18] For the η-phase very few reports about a preparation from Mn + N_2 exist.[19] The synthesis route used here confirms that this is indeed possible.

The η-phase is commonly referred to as η-Mn_3N_2. In this formula 2/3 of the octahedral sites are occupied by N. This occurs in such an ordered way that two inequivalent Mn sites result. One is coordinated twofold and the other fivefold by N (Fig. 1). The unit cell of the superstructure contains three fcc unit cells. This ordering pattern of N—as derived from X-ray powder diffraction—was for the first time reported in a review[2] citing a conference abstract.[20] However, experimental details were not given.

Without knowledge of these works the crystal structure of η-Mn_3N_2 was redetermined by X-ray diffractometry on single crystals grown from supercritical ammonia.[21] Neutron powder diffraction data[8] confirmed the ordering of N and established an antiferromagnetic superstructure as given in Fig. 1. The crystallographically distinct Mn sites carry magnetic moments of different magnitudes (Table 1). The overall magnetic structure is antiferromagnetic of the first kind,[22] *i.e.* ferromag-

†Present address: Max-Planck-Institut für Metallforschung, Seestraße 92, 70174 Stuttgart, Germany.

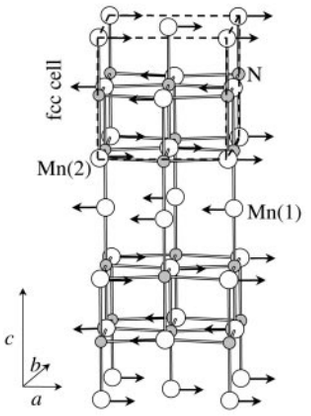

Fig. 1 Nuclear and spin structure of η-Mn_3N_2 given for one unit cell in a face-centred tetragonal setting. The arrows represent the magnetic moments according to the antiferromagnetic structure of the first kind. The dashed lines indicate the pseudo-cubic unit cell of the rocksalt type.

Table 1 Nuclear and spin structure of η-Mn_3N_2 as obtained from a previous neutron diffraction study at ambient temperature.[8] Space group type of nuclear structure: *F*4/*mmm*, $a = 4.200(1)$ Å, $c = 12.129(4)$ Å, the magnetic space group is $F_C mm'm'$

Atom	*x*	*y*	*z*	$\mu_{m,x}/\mu_B$
Mn(1)	0	0	0	4.4(5)
Mn(2)	0	0	0.333(1)	3.4(2)
N	0	0	0.1588(6)	—

netic layers in (001) are coupled antiferromagnetically along [001]. The magnetic moments are oriented perpendicular to [001]. The magnetic susceptibility of η-Mn_3N_2 below ambient temperatures shows the behaviour of a Pauli paramagnet.[8] However, measurements at $T \leqslant 1000$ K show a maximum of susceptibility at about 913–923 K indicating the Néel temperature.[23] DSC[21] and DTA[23] investigations indicate an endothermic effect at similar temperatures.

The X-ray diffraction patterns of the η- and θ-phases are very similar, but the two phase field η/θ was clearly established.[24] The θ-phase is often referred to as θ-Mn_6N_5, which corresponds roughly to the lower compositional limit. However, this formula cannot be related to an ordered superstructure of N of that particular composition. In fact, in several investigations concerning the crystal structure of the θ-phase—performed using X-ray diffraction data on powders,[20] on *c*/*a* twinned "single crystals"[8,25] or by using electron diffraction on powders[26]—no hints of long-range order of N were observed. Nevertheless, the unfavourable ratio of the scattering powers of Mn and N makes it possible that weak superstructure reflections were missed in these studies. A recently reported MnN produced by DC reactive sputtering was characterised by X-ray diffraction and magnetometry.[27] Crystallographic data indicate that this material belongs to the θ-phase with, however, unexpected large lattice constants. The magnetic properties are similar to those reported previously[23] for θ-phase materials.

High temperature electron diffraction[26] revealed a probably continuous phase transition for θ-manganese nitrides of various compositions: the cell dimensions change continuously from face-centred tetragonal to face-centred cubic at about 700 K. There are values reported for different N contents, however no simple trend results as a function of composition. This phase transition explains *c*/*a* twinning of the crystals of the θ-phase which were grown above 700 K in supercritical ammonia.[8,25]

There are hints that the two-phase field η + θ disappears at elevated temperatures:[28] Mn powder was nitrided at 870 K with varying nitridation atmospheres (NH_3/H_2 ratio) and then

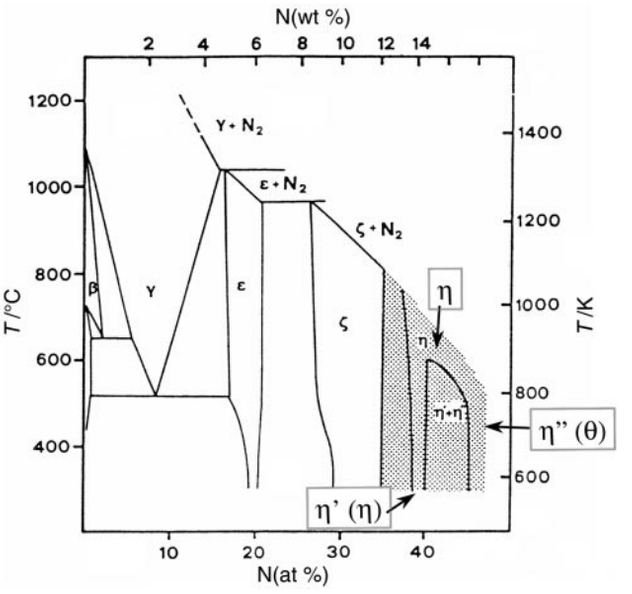

Fig. 2 Phase diagram Mn/N as suggested in the literature.[28] The proposed single η-phase field which splits below roughly 870 K into the η- and θ-phase (called η′ and η″) is shaded. We come to slightly different conclusions with respect to this field.

quenched to ambient temperature. The resulting reaction products had a tetragonally distorted fcc structure of Mn and showed—as a function of N content—a continuous variation of cell parameters from typical values of the η-phase to those of the θ-phase. Only subsequent annealing at 670–770 K resulted in phase separation into η- and θ-phases of higher and lower N content. From these results a modified phase diagram was suggested (Fig. 2) containing one single η-phase field with a critical point. Motivated by this, the authors referred to the η- and the θ-phase as η′ and η″.

This, however, does not take into account the presence of ordering of N in the η-phase as well as the observed phase transitions for both the η- and the θ-phase.

We now analysed the distribution of N and the magnetic structure within the θ-phase using neutron diffraction. Furthermore, the phase transition tetragonal–cubic at about 700 K was studied in order to clarify a possible interplay between changes in cell dimensions and magnetic ordering in the θ-phase. For comparison we re-examined the crystal and magnetic structures of η-Mn_3N_2 at ambient temperatures. DSC investigations accompanied the neutron diffraction studies.

Experimental

Preparation and characterization

η-Mn_3N_2 was prepared from manganese (Fluka AG, Buchs, CH, >99% contains 0.2 wt.% O, particle size 0.3 mm) and NaN_3 (Fluka Chemie, Neu-Ulm, D, >99.9%). 4–10 g Mn were reacted with an excess of 20% of NaN_3—with respect to the formation of Mn_3N_2—in steel autoclaves.[29] The autoclave was filled under an inert Ar atmosphere[30] and heated to 750 °C for 6 d. It was cooled by switching off the furnace. A high residual N_2 pressure was released from the autoclave when opened. The crude product consisted of η-Mn_3N_2 in a matrix of Na metal produced from thermal decomposition of the NaN_3. The material was carefully brought into EtOH to remove Na. Then the residual material was washed with water, aqueous NH_4Cl solution, filtered, again washed with water, EtOH and Et_2O, and finally dried in vacuum. Guinier powder patterns (FR552, Enraf-Nonius Delft, NL; CuKα_1 radiation; corrected using Si standard) of the final product showed only reflections of

η-Mn_3N_2 (face-centred tetragonal, three superstructure reflections of the ordered N arrangement are observed, $a=4.205(1)$ Å, $c=3\times4.041(1)$ Å). Elemental analysis (combustion analysis, TC436DR, LECO, St. Joseph, USA) gave 14.2(1)% N and 0.30(2)% O. We treated the O content to be present as MnO—although this is not observed in the diffraction patterns (see below)—and calculated a "corrected" N content of the nitride of $Mn_3N_{1.97}$. There are no hints of the formation of a ternary sodium manganese nitride under these reaction conditions. For Mn powder with this particle size (0.3 mm) typically 0.1–0.3 wt.% Na were found in the final product (ICP-OES, Vista RL, Varian, Melbourne, AUS). Considerably more O and Na was found if an Mn powder of smaller particle size (<0.1 mm as used for preparation of the θ-phase material) is used as the starting material.

θ-Phase material was prepared from manganese powder (Merck, Darmstadt, 99.9%, particle size <0.1 mm) by nitriding it at 600 °C for 12 h with flowing NH_3. NH_3 was dried over sodium at 8 bar before feeding it into the apparatus. From Guinier powder patterns cell parameters of the θ-phase of $a=4.219(1)$ Å and $c=4.129(1)$ Å resulted. Furthermore, tiny reflections of MnO were observed. Elemental analysis gave an N content of 18.5(1) wt.% and an O content of 0.20(2) wt.%. Correcting for the MnO content the composition of the pure nitride is $Mn_6N_{5.40}$. However, we will refer to the θ-phase material as θ-$Mn_6N_{5.26}$ as this composition results from the refinement of N content from neutron diffraction data taken at ambient temperature (see below).

It is confusing that the O content in the η-Mn_3N_2 material does not give rise to reflections of MnO as an even smaller content does for θ-$Mn_6N_{5.26}$. Possibly, the oxygen impurities detected in the η-Mn_3N_2 material result from poorly crystalline ternary sodium manganese oxides or from manganese hydroxides formed during the preparation or the work-up procedure. In fact, annealing the η-Mn_3N_2 at 500 °C for 2 d gives rise to MnO reflections. We did not intend to study this in further detail.

Neutron diffraction

The samples were placed into cylindrical vanadium containers. The container for θ-$Mn_6N_{5.26}$ was only loosely closed in order to prevent destruction by the irreversible evolution of N_2 from the material that had to be considered at elevated temperatures.[25]

Neutron diffraction experiments were performed using the time-of-flight diffractometer ROTAX installed at the pulsed spallation neutron source ISIS in the Rutherford Appleton Laboratory, UK. Data were recorded independently on two or three different detector banks covering different ranges of *d*-spacings (for details see results of Rietveld refinements).

Increased sample temperatures were generated by a furnace with a vanadium shield and a continuously evacuated sample chamber. A manometer allowed us to monitor the possible evolution of N_2 from decomposition of the sample.

Rietveld refinement

For Rietveld refinement the GSAS package of programs[31] was used. It allows simultaneous evaluation of the data recorded on the different detector banks. Although refinement was carried out using all data we will only show the profile fits of the forward scattering bank as they reveal all the important features discussed in the text.

The nuclear scattering lengths used were $b(\mathrm{Mn})=0.373\times10^{-12}$ cm and $b(\mathrm{N})=0.936\times10^{-12}$ cm.[32] The magnetic form factor of Mn^{2+} was expressed by $f(\sin\theta/\lambda)=\Sigma A_i\exp(-B_i(\sin\theta/\lambda)^2)+C$ with $i=1, 2, 3$.[33] The coefficients of the Mn^{2+} ion form factor were taken as they gave the best results in a previous neutron diffraction study on η-Mn_3N_2.[8] The background of the diffraction patterns was fitted using shifted Chebichev polynomials. The appropriate number of terms was optimised for each detector bank. The reflection profiles were fitted by an exponential pseudo-Voigt convolution as implemented in the GSAS package. Absorption due to the sample and its environment was empirically refined with a model for linear absorption. This was independently done for each bank for the measurements on both nitrides at ambient temperatures. For the high temperature experiments on the θ-phase the absorption parameter for each of the three detector banks was determined from a simultaneous refinement of the data taken at 473 K and 598 K. These parameters were used for all final refinements of the high temperature data. The presence of MnO in our θ-$Mn_6N_{5.26}$ sample was considered by a two phase refinement. Thermal parameters of Mn and O in MnO were constrained to the values of Mn and N for the nitride.

DSC measurements

DSC experiments on η-Mn_3N_2 were performed on a DSC2 (Perkin-Elmer, Überlingen, D), using cold-welded silver crucibles. Measurements on θ-$Mn_6N_{5.26}$ were done on a DSC 204 Phoenix (Netzsch, Selb, D). Owing to the nitrogen evolution at higher temperatures Au coated pressure crucibles made from Cr–Ni steel with an AuCu seal were used ($p_{max}=100$ bar, $T_{max}=773$ K).

Results

We will first present the results of the neutron diffraction experiments on η-Mn_3N_2 and θ-$Mn_6N_{5.26}$ at ambient temperature. Then we will report the results of DSC measurements. Finally, we analyse the high temperature neutron diffraction studies on θ-$Mn_6N_{5.26}$.

Neutron diffraction of η-Mn_3N_2 at ambient temperature

The starting points for the re-evaluation of the nuclear and spin structures of η-Mn_3N_2 are the previously reported data.[8] These are given in Table 1 and may be directly related to Fig. 1. In advance of the evaluation of the new data some comments are required concerning the spin structure: Keeping the configurational symmetry, *i.e.* the relative orientations of collinear magnetic moments, magnetic structural models with different directions of the magnetic moments within the (001) plane of the tetragonal unit cell are indistinguishable from diffraction data from powders.[34] Therefore, the solution arbitrarily chosen by us, which is $\boldsymbol{\mu}_m \parallel [100]$ with a magnetic symmetry $F_Cmm'm'$, is only one of two high symmetric solutions; the other is $\boldsymbol{\mu}_m \parallel [110]$. All directions within (001) are only allowed when the magnetic symmetry is reduced to monoclinic.

Furthermore, if the positional parameter of Mn(2) is at its ideal value of $z(\mathrm{Mn}(2))=1/3$ and differences between the Debye–Waller factors of Mn(1) and Mn(2) are neglected, the structure factors of two classes of magnetic reflections are

$$|F|^2(h,k,l)\propto(\mu_m(\mathrm{Mn}(1))+2\mu_m(\mathrm{Mn}(2)))^2=(3p)^2 \qquad \text{for } l=3n \tag{1}$$

$$|F|^2(h,k,l)\propto(\mu_m(\mathrm{Mn}(1))-\mu_m(\mathrm{Mn}(2)))^2=q^2 \qquad \text{for } l\neq3n \tag{2}$$

The parameters p and q can be interpreted as the mean magnitude of the magnetic moments (magnetisation per metal atom in the magnetically ordered state) of Mn—weighted by the different frequencies of Mn(1) and Mn(2) within the unit cell—and the difference of the two different magnetic moments. This is in fact the direct information which results from the diffraction patterns as the phase information of the structure factors is not available. In the case of nearly equal magnitudes of the moments for Mn(1) and Mn(2) magnetic superstructure

reflections $l \neq 3n$ are expected to be very weak compared to those with $l = 3n$. According to eqn. (2) q is either

$$\mu_m(\mathrm{Mn}(1)) - \mu_m(\mathrm{Mn}(2)) = q \quad (3)$$

or

$$-\mu_m(\mathrm{Mn}(1)) + \mu_m(\mathrm{Mn}(2)) = q \quad (4)$$

As a consequence, the two alternatives for the magnetic moments of the different Mn sites are

$$\mu_m(\mathrm{Mn}(1)) = p + 2/3q \quad \text{and} \quad +\mu_m(\mathrm{Mn}(2)) = p - 1/3q \quad (5)$$

or

$$\mu_m(\mathrm{Mn}(1)) = p - 2/3q \quad \text{and} \quad +\mu_m(\mathrm{Mn}(2)) = p + 1/3q \quad (6)$$

These solutions are—under the above mentioned assumptions—indistinguishable from powder diffraction patterns.

The neutron diffraction patterns of η-Mn_3N_2 taken at ambient temperatures (Fig. 3) show the same reflections as were reported previously.[8,25] However, the range of d-values accessible is now larger, both to lower and higher values, *e.g.* the magnetic superstructure reflection (001) at $d = 12.1$ Å is detected. A visual analysis of the diffraction patterns shows that (001) is the only reflection with $l \neq 3n$ which is observed with significant intensity.

The overall details and results of the Rietveld refinement of the neutron diffraction data of η-Mn_3N_2 are summarised in Table 2. The two possibilities for the magnetic structure according to eqn. (5) and (6) give the same residuals. The mean magnetic moment of Mn, $p = 3.6\ \mu_B$, is in good agreement with the previously reported value of 3.7 μ_B.[8,25] However, the value of q, the difference of the magnetic moments of Mn(1) and Mn(2) (0.3 μ_B), is considerably smaller than the value of 1 μ_B. In fact, we analysed the old diffractograms[8,25] and realised that the $l \neq 3n$ magnetic reflections were not observed at all with significant intensity. Therefore, it has to be concluded that the value of 1 μ_B was an artefact of the Rietveld refinement and the two moments for Mn(1) and Mn(2) were highly correlated.

Note that the value of q resulting from this study is very sensitive to possible systematic errors in the diffraction data and their refinement: q is mainly extracted from the intensity of the (001) reflection recorded at a very high d-value. There are no other reflections within a large region of d-spacings, as the next reflection (002) has half its d-value (compare Fig. 3). This fact makes it difficult to detect systematic errors, *e.g.* inadequate refinement of absorption. However, considerably higher values of q should have caused significant magnetic superstructure reflection intensities for $l \neq 3n$ also at lower d-values.

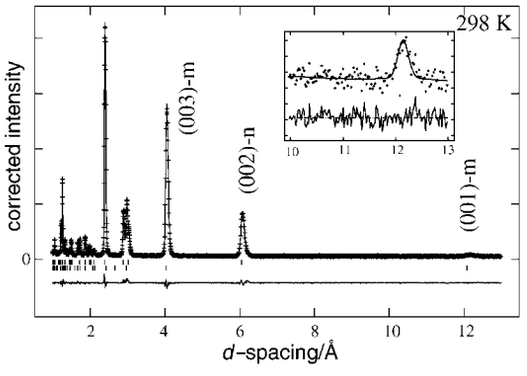

Fig. 3 η-Mn_3N_2: Neutron diffraction data (forward scattering detector bank) taken at ambient temperatures fitted by Rietveld refinement and displaying the difference curve. Reflection markers: nuclear structure (top line), magnetic structure (bottom). Certain reflections are labelled by (*hkl*) with n indicating nuclear and m magnetic reflections. The magnetic reflection (001) containing the information about the difference of the magnetic moments of the different Mn sites is given enlarged in the inset.

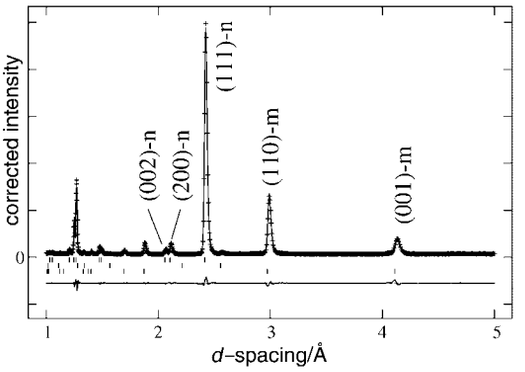

Fig. 4 θ-$Mn_6N_{5.26}$: Neutron diffraction data (forward scattering detector bank) taken at ambient temperatures fitted by Rietveld refinement and displaying the difference curve. Reflection markers: nuclear structure (top line), MnO (middle), magnetic structure (bottom). Certain reflections are labelled by (*hkl*) with n for nuclear and m for magnetic reflections.

Neutron diffraction on θ-$Mn_6N_{5.26}$ at ambient temperatures

The diffraction patterns of θ-$Mn_6N_{5.26}$ taken at ambient temperatures show the reflections already visible in X-ray patterns but also some new reflections violating the extinction rules for a face-centred unit cell (Fig. 4). These correspond to the strong magnetic reflections with $l = 3n$ found for η-Mn_3N_2. Therefore, one finds again an antiferromagnetic structure of the first kind, *i.e.* a ferromagnetic coupling between the spins within the (001) planes and antiferromagnetic coupling along the [001] direction.

Rietveld refinements (Table 2) were performed on the basis of a defect-NaCl type structure with tetragonal distortion as well as with the above mentioned antiferromagnetic structure of the first kind. Such a model was sufficient to attain a convincing fit of the diffraction data. Therefore, no evidence remains for long-range ordering of N on the octahedral sites.

Refinements of the occupancy of the N site finally resulted in the composition $Mn_6N_{5.26}$. The N content is 2.5% less than the value resulting from elemental analysis ($Mn_6N_{5.40}$); however, both are considerably larger than the "nominal" composition Mn_6N_5. The relation between N content and cell parameters has been examined[24] and mathematically evaluated. With these data the cell parameters a and c lead to compositions $Mn_6N_{5.26}$ and $Mn_6N_{5.23}$ respectively. As c varies much more markedly with the N content than a,[24] $Mn_6N_{5.26}$ is to be preferred. Therefore, in the following we refer to the composition $Mn_6N_{5.26}$.

In contrast to η-Mn_3N_2 a refinement of the orientation of the magnetic moments relative to [001] was necessary for θ-$Mn_6N_{5.26}$. An arbitrary direction of collinear magnetic moments within the fcc unit cell can be achieved using the magnetic space group F_C2'/m'.[35] The results of the refinements indicate that the direction of the collinear magnetic moments is tilted by 22° from the tetragonal c axis (Table 2, Fig. 5). As pointed out above for η-Mn_3N_2 the direction of the component of the magnetic moments within the (001) plane cannot be determined from neutron powder diffraction data.

Thermal analysis of the phase transitions in η-Mn_3N_2 and θ-$Mn_6N_{5.26}$

DSC investigations on η-Mn_3N_2 and θ-$Mn_6N_{5.26}$ confirmed the phase transitions for both compositions.[21,23,26]

η-Mn_3N_2 exhibits a sharp, reversible and reproducible signal

Table 2 Results of Rietveld refinement on neutron diffraction data of η-Mn_3N_2 and θ-$Mn_6N_{5.26}$ taken at ambient temperature. Data separated by a "/" refer to the two different multidetector banks used

Substance	η-Mn_3N_2	θ-$Mn_6N_{5.26}$
Detector angles/°	45/122	45/122
No. of background parameters	12/8	12/12
No. of profile parameters	5/3	5/3
Minimal *d*-value considered in the Rietveld refinements:		
Nuclear structure		
d_{min}/Å	0.49/0.3	0.49/0.3
Magnetic structure		
d_{min}/Å	1.0/1.0	1.0/1.0
Cell parameters:		
a/Å	4.2046(1)	4.2193(1)
c/Å	12.124(1)	4.1287(1)
	$=3\times4.041$	
	$c/(3a)=0.9612$	$c/a=0.9785$
Space group type for nuclear structure	*F*4/*mmm*	*F*4/*mmm*
Positional parameters:		
Mn(1)	0 0 0	0 0 0
Mn(2)	0 0 0.3333(1)	
N	0 0 0.15963(5)	0 0 1/2
Occupancy for N site	1	0.877(4)
$100u_{Mn(1)}$/Å^2	0.70(3)	0.41(2)
$100u_{Mn(2)}$/Å^2	0.34(2)	
$100u_N$/Å^2	0.54(1)	0.72(2)
Magnetic space group type	$F_C mm'm'$	$F_C 2'/m'$
Magnetic moments/μ_B	$\mu_{m,x}(Mn(1))=3.75(1)$	$\mu_{m,x}(Mn)=1.28(1)$
	$\mu_{m,x}(Mn(2))=3.47(1)$	$\mu_{m,z}(Mn)=3.06(2)$
	or	$\mu_m=3.31(2)$
	$\mu_{m,x}(Mn(1))=3.38(1)$	
	$\mu_{m,x}(Mn(2))=3.65(1)$	
Tilting angle of the magnetic moments relative to [001]/°	90	22.7(2)
Cell parameter MnO, *a*/Å	—	4.4441(7)
Phase content MnO [%]	—	1.08(5)[a]
wR_P	4.9/5.5	4.8/5.3
$R_{B,nucl}(F^2)$	4.1/6.5	5.4/8.2
$R_{B,magn}(F^2)$	4.7/16	11/14

[a]Related to number of Mn atoms.

at $T_{onset}=927$ K and 916 K for heating and cooling, respectively. The enthalpy (median value of different measurements) is 8.2 kJ mol^{-1} (referring to a formula unit $MnN_{0.67}$).

The transition of θ-$Mn_6N_{5.26}$ occurs at $T_{onset}=665$ K without any noticeable hysteresis. Initial measurements in cold welded Al pans indicated an irreversible evolution of nitrogen at higher temperatures as the pans inflated. A sample examined after the DSC measurements by taking a Guinier film pattern showed cell parameters of $a=4.220$ Å and $c=4.214$ Å which yield[16,24] compositions of $Mn_6N_{5.17}$ and $Mn_6N_{5.19}$, respectively.

Fig. 6 shows the resulting curves on heating and cooling of three consecutive measurements of the identical sample θ-$Mn_6N_{5.26}$ ($T_{max}=773$ K) performed in pressure resistant crucibles. The initial signal appears to consist of three broad peaks also visible in the first transition on cooling. Further measurements result in sharper signals with a two peak structure, shifted to somewhat lower temperatures. An enthalpy of roughly 1.4 kJ mol^{-1} (referring to $MnN_{0.88}$) results if a first order character is assumed. If the transition is, however, of second order character one only detects the maximum of C_p and the transition enthalpy given above has no well defined physical meaning.

From these data we currently can not give a full interpretation of the multipeak structure of the signal, nor a definite statement whether the transition is of first or second order.

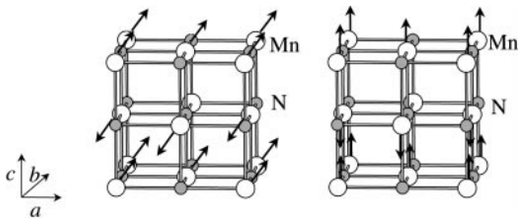

Fig. 5 Unit cell of θ-$Mn_6N_{5.26}$ indicating its nuclear and spin-structure in an analogous way as for η-Mn_3N_2 (Fig. 1). The N sites are only partially occupied: Ambient temperature (left); just below the phase transition at about 665 K (right).

High temperature neutron diffraction on θ-$Mn_6N_{5.26}$

High temperature neutron diffraction experiments on θ-$Mn_6N_{5.26}$ were performed for $323\text{ K}\leqslant T\leqslant673$ K including a heating and a cooling period (see Table 3 for particular sample temperatures). Fig. 7 shows diffraction patterns from

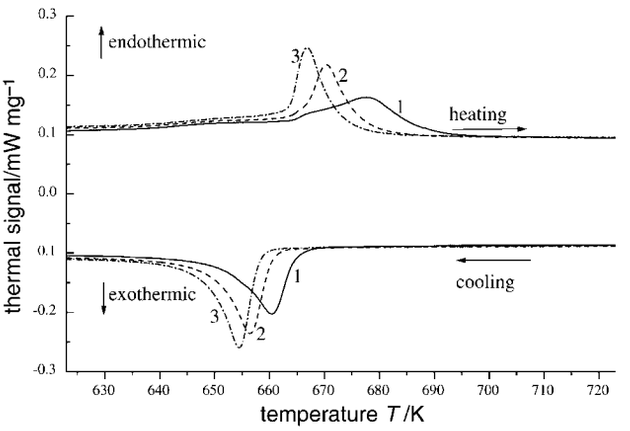

Fig. 6 DSC heating and cooling curves for θ-$Mn_6N_{5.26}$ (5 K min^{-1}). The cycles are numbered.

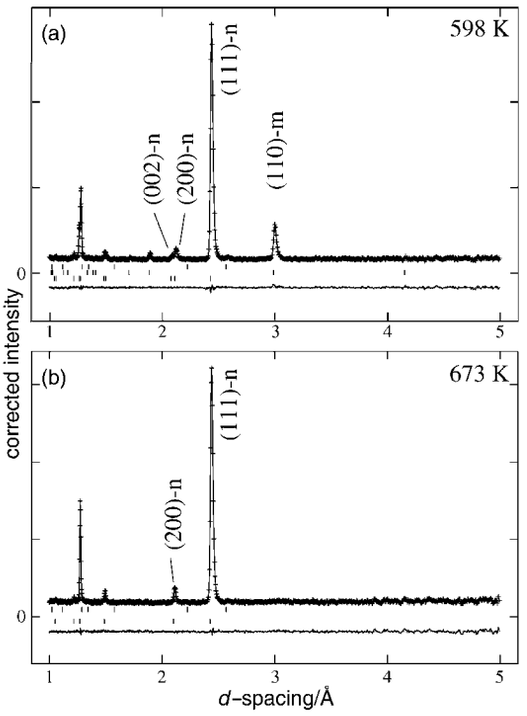

Fig. 7 θ-$Mn_6N_{5.26}$: High temperature neutron diffraction patterns (forward scattering bank) taken at 598 K (top), 673 K (bottom) as fitted by Rietveld refinement and displaying the difference curve. Reflection markers: nuclear structure (top line), magnetic structure (middle; not included for 673 K), MnO (bottom). Certain reflections are labelled by (*hkl*) with n for nuclear and m for magnetic reflections.

the heating period at 598 K and 673 K. Compared to the situation at ambient temperatures (Fig. 4) we find a strong decrease of the intensity of the magnetic superstructure reflection (001) at elevated temperatures. It disappears in the range of temperatures $548 \leqslant T \leqslant 598$ K. Above 598 K this reflection is absent. In correspondence to the angular dependence of magnetic scattering the structure factor of the reflection (001) contains the magnetic component within the *ab*-plane of the tetragonal unit cell. The absence of this reflection can be interpreted by an alignment of the magnetic moments along [001]. This corresponds to an increase of magnetic space group symmetry from F_C2'/m' to $F_C4/mm'm'$.

At 673 K all magnetic reflections have disappeared as well as the splitting of the reflections, *e.g.* (200) and (002) (Fig. 7). This means that the material has become face-centred cubic without any magnetic superstructure. During the data collection at this temperature we registered a slight increase of pressure in the evacuated sample chamber of the furnace. This indicates—as already found in the DSC measurements—a decomposition of the sample under evolution of N_2. The decomposition apparently stops when the temperature is reduced.

During the cooling period the temperature range for $F_C4/mm'm'$ symmetry is $503\ \text{K} \leqslant T \leqslant 623$ K. It is extended to lower temperatures compared to the experiments while heating. At even lower temperatures the reflection (001) reappears. During the high temperature measurements the reflections of MnO were always visible and its amount did not change significantly.

In all refinements of the high temperature data the occupancies of N on the octahedral sites were kept constant at the value $Mn_6N_{5.26}$ as determined for the ambient temperature data. After the apparent loss of nitrogen at high temperatures there is no evidence that this affects the parameters of the nuclear structure significantly, *e.g.* the occupancy of N. Table 3 summarises the results of the Rietveld refinements.

In Fig. 8 the magnitude of the magnetic moments as well as their angle relative to [001] are plotted as a function of temperature for the heating and the cooling period.

Discussion

Both η-Mn_3N_2 and θ-$Mn_6N_{5.26}$ are interstitial compounds based on an fcc type arrangement of Mn atoms. Neutron diffraction data at ambient temperatures reveal a collinear antiferromagnetic superstructure of the first kind accompanied by a tetragonal distortion of the cell dimensions for both compounds. In η-Mn_3N_2 the arrangement of N on the octahedral sites is ordered which causes two crystallographically distinct Mn sites. These carry slightly different magnetic moments ($\Delta\mu = 0.3\ \mu_B$). This has no marked influence on the overall antiferromagnetic superstructure.

The magnetic structures of η-Mn_3N_2 and θ-$Mn_6N_{5.26}$ as

Table 3 Results of Rietveld refinements of neutron diffraction experiments on θ-$Mn_6N_{5.26}$ at elevated temperatures. The symmetry of the nuclear structure is $Fm\bar{3}m$ at 673 K (Mn: 0 0 0, N: 1/2 0 0, occupancy 0.877 as resulting for ambient temperatures) and *F*4/*mmm* (Mn: 0 0 0, N: 1/2 0 0, occupancy 0.877) at the other temperatures. Measuring temperatures are given in the temporal succession. Three detector banks were at 45°/90°/136° with minimal *d*-values of data considered for refinements 0.51 Å/0.50 Å/0.50 Å. Profile parameters were 5/2/2, background parameters 24/10/16

T/K	*a*, *c*/Å	$100u$/Å^2 Mn, N	Space group type of magnetic structure	$\mu_{m,x}$, $\mu_{m,z}/\mu_B$	μ_m/μ_B	$\alpha(\mu_m,c)$/°
323	4.2187(1)	0.57(2)	F_C2'/m'	1.24(2)	3.130(8)	23.4(4)
	4.1288(1)	0.82(1)		2.872(9)		
473	4.2282(1)	0.80(2)	F_C2'/m'	0.75(3)	2.81(1)	15.5(6)
	4.1419(1)	1.10(1)		2.71(1)		
548	4.2317(1)	0.97(3)	F_C2'/m'	0.49(5)	2.45(1)	11(1)
	4.1530(1)	1.21(2)		2.49(1)		
598	4.2324(1)	1.09(3)	$F_C4/mm'm'$	0(—)	2.27(1)	0(—)
	4.1643(1)	1.30(2)		2.27(1)		
673	4.2153(1)	1.28(3)	$Fm3m1'$	0(—)	0(—)	0(—)
		1.54(2)		0(—)		
648	4.2285(1)	1.16(3)	$F_C4/mm'm'$	0(—)	1.68(1)	0(—)
	4.1819(1)	1.45(2)		1.68(1)		
623	4.2311(1)	1.06(4)	$F_C4/mm'm'$	0(—)	2.04(1)	0(—)
	4.1705(1)	1.40(2)		2.04(1)		
573	4.2319(1)	0.95(3)	$F_C4/mm'm'$	0(—)	2.430(9)	0(—)
	4.1570(1)	1.28(2)		2.430(9)		
503	4.2303(1)	0.88(2)	$F_C4/mm'm'$	0(—)	2.734(9)	0(—)
	4.1446(1)	1.13(1)		2.734(9)		
423	4.2257(1)	0.74(2)	F_C2'/m'	0.61(4)	2.94(1)	11.9(8)
	4.1361(1)	0.99(1)		2.87(1)		
323	4.2194(1)	0.57(2)	F_C2'/m'	1.00(3)	3.124(9)	18.7(5)
	4.1281(1)	0.83(1)		2.96(1)		

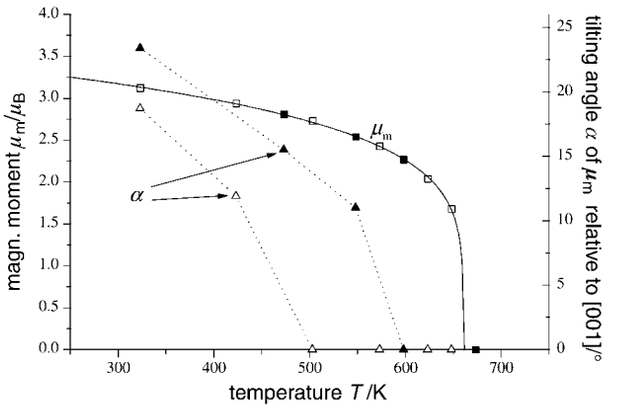

Fig. 8 θ-$Mn_6N_{5.26}$: Dependence of the overall magnetic moment (squares) and its tilting angle to [001] (triangles) on the temperature (full markers: heating period, open markers: cooling period). The function $\mu_m(T)$ is plotted as fitted under the assumption of critical behaviour (no details given), the values for the angles are only connected as a guide for the eye.

observed at ambient temperatures differ mainly by the orientations of the magnetic moments relative to the tetragonal unit cells. Whereas the strong exchange interactions are similar in these phases as both have an antiferromagnetic structure of the first kind, weaker anisotropy interactions most likely determine the particular orientations of the ordered magnetic moments relative to the crystal lattice.[22]

θ-$Mn_6N_{5.26}$ shows two phase transitions when heated to elevated temperatures. The first occurs, according to our neutron diffraction experiments, between 548 K and 598 K for the heating and between 503 K and 423 K for the cooling period (see preceding section). This transition involves only an alignment of the overall magnetic moments along the direction [001]. In the corresponding ranges of temperatures the overall ordered magnetic moments μ_m and the lattice parameters vary continuously and show no large differences for the heating and cooling period. The discrepancies in the transition temperatures for the alignment of the ordered magnetic moments along [001] may be attributed to the slight loss of N_2 which was however not detected by chemical analysis and changes of cell parameters at ambient temperatures after the measurement.[36] However, weak anisotropy interactions may be influenced by a small loss of N_2 without marked effects on the stronger exchange interactions. These determine the antiferromagnetic structure of 1st kind and the magnitude of the ordered moments which remain virtually unchanged.

The second phase transition in θ-$Mn_6N_{5.26}$ is detected by DSC measurements and by neutron diffraction. It occurs at about 660 K and involves an apparently continuous decay of the magnetic moments resulting in a paramagnetic and cubic high temperature phase. Therefore, this transition corresponds to the Néel point. There are no hints that order–disorder phenomena of N on octahedral sites are related to the changes of the lattice. Obviously, the changes of magnetic structure are responsible for the structural distortions. The effects observed for θ-$Mn_6N_{5.26}$ are similar to the behaviour of the interstitial compound CrN.[12] Its high temperature phase has an NaCl type structure. In the low temperature phase an orthorhombic distortion of the unit cell dimensions is found. As the octahedral sites are fully occupied no order–disorder transition concerning N is possible.

The phase transition of η-Mn_3N_2 detected at about 913–923 K by DSC measurements may be interpreted—as well as the second transition of θ-$Mn_6N_{5.26}$—as an antiferromagnetic–paramagnetic phase transition. However, the thermal effect for η-Mn_3N_2 is much stronger than that for θ-$Mn_6N_{5.26}$, yielding thermodynamic factors[37] of 3 for η-Mn_3N_2 compared with 1.1 for θ-$Mn_6N_{5.26}$. For η-Mn_3N_2 this may indicate a contribution of a disordering of N at the transition temperature. This would result in a disordered and paramagnetic high temperature phase of η-Mn_3N_2 which is of the same symmetry as the high temperature phase of θ-$Mn_6N_{5.26}$. This view is supported by quenching experiments,[28] which have been interpreted in terms of a continuous solid solution of η-Mn_3N_2 and θ-$Mn_6N_{5.26}$ at high temperatures. However, the presence of a simple critical point terminating the two phase area η/θ to high temperatures[28] has to be rejected as both corresponding crystal structures are not isotypic. The results obtained here allow the development of a refined picture: Both the η- and the θ-phase probably have a common high temperature phase, which is paramagnetic and cubic with a disordered distribution of the N atoms on the octahedral sites. There is a general tendency to form an antiferromagnetic superstructure of the first kind for a wide range of compositions. η-Mn_3N_2 may, therefore, be regarded as a special case of a θ-phase with ordered arrangement of N.

The magnetic and structural behaviour observed for the manganese nitrides show strong similarities to certain Mn alloys with other elements (Cu, Ni, Fe, Ge, Pd, Au).[38] These elements may stabilise the γ-Mn modification of the fcc structure. At low temperatures these alloys form antiferromagnetic structures of the first kind accompanied by a tetragonal distortion of the crystal lattice. Magnetic order and tetragonal distortion disappear at the same or slightly different temperatures in a first or second order manner. If both phase transitions occur continuously at the same temperature one may speak of a pseudo-martensitic phase transition in order to stress the difference from an "ordinary" martensitic phase transition, which is essentially of first order character.[38]

Acknowledgements

We thank Ulrike Schmidt (MPI CPfS Dresden) for performing chemical analyses. Financial support by the "Bundesministerium für Bildung, Wissenschaft, Forschung und Technologie" (JA5DOR and KI5BO3), the "Deutsche Forschungsgemeinschaft" and the "Fonds der Chemischen Industrie" is gratefully acknowledged.

References

1 R. Juza, *Adv. Inorg. Chem. Radiochem.*, 1967, **9**, 81.
2 D. H. Jack and K. H. Jack, *Mater. Sci. Eng.*, 1973, **11**, 1.
3 G. Hägg, *Z. Phys. Chem. Abt. B*, 1931, **12**, 33.
4 G. E. Bacon, *Neutron Diffraction*, 3rd edn., Clarendon Press, Oxford, 1975.
5 A. N. Christensen and B. Lebech, *Acta Crystallogr., Sect. B*, 1979, **35**, 2677.
6 M. Nasr Eddine, E. F. Bertaut and M. Maunaye, *Acta Crystallogr., Sect. B*, 1977, **33**, 2696.
7 M. Mekata, J. Haruna and H. Takaki, *J. Phys. Soc. Jpn.*, 1968, **25**, 234.
8 G. Kreiner and H. Jacobs, *J. Alloys Compd.*, 1992, **183**, 345.
9 A. Leineweber, H. Jacobs, F. Hüning, H. Lueken, H. Schilder and W. Kockelmann, *J. Alloys Compd.*, 1999, **288**, 77.
10 D. Rechenbach and H. Jacobs, *J. Alloys Compd.*, 1996, **235**, 15.
11 A. Leineweber, H. Jacobs, W. Kockelmann and S. Hull, *Physica B*, 2000, **276–278**, 266.
12 L. M. Corliss, N. Elliot and J. M. Hastings, *Phys. Rev.*, 1960, **117**, 929.
13 W. J. Takei and G. Shirane, *Phys. Rev.*, 1960, **119**, 122.
14 M. Nasr Eddine and E. F. Bertaut, *Solid State Commun.*, 1977, **23**, 147.
15 B. C. Frazer, *Phys. Rev.*, 1958, **112**, 751.
16 N. A. Gokcen, *Bull. All. Phase Diagrams*, 1990, **11**, 33.
17 E. Lehrer, *Z. Elektrochem.*, 1930, **36**, 383.
18 M. Katura, *J. Alloys Compd.*, 1992, **182**, 91.
19 Y. Imai and T. Masumoto, *Sci. Rept. Inst. Tohoku Univ. A*, 1964, **16**, 31.
20 K. H. Jack, *The Mechanism of Phase Transformations in Crystalline Solids*, Institute of Metals, London, 1968, p. 221.

21 H. Jacobs and C. Stüve, *J. Less-Common Met.*, 1984, **96**, 323.
22 E. Jäger and R. Perthel, *Magnetische Eigenschaften von Festkörpern*, Akademie-Verlag, Berlin, 1996.
23 M. Tabuchi, M. Takahashi and F. Kanamura, *J. Alloys Compd.*, 1994, **210**, 143.
24 F. Lihl, P. Ettmayer and A. Kutzelnigg, *Z. Metallk.*, 1962, **53**, 715.
25 G. Kreiner, Dissertation, Universität Dortmund, 1991.
26 N. Otsuka, Y. Hanawa and S. Nagakura, *Phys. Status Solidi A*, 1977, **43**, K127.
27 K. Suzuki, T. Kaneko, H. Yoshida, Y. Obi, H. Fujimori and H. Morita, *J. Alloys Compd.*, 2000, **306**, 66.
28 A. Burdese, D. Firrao and M. Rosso, *Metall. Sci. Technol.*, 1994, **2**, 43.
29 Th. Brokamp, Dissertation, Universität Dortmund, 1991.
30 H. Jacobs and D. Schmidt, *Curr. Top. Mater. Sci.*, 1982, **8**, 379.
31 A. C. Larson and R. B. von Dreele, *GSAS-General Structure Analysis System Manual*, Los Alamos, 1994.
32 V. F. Sears, Internal report AECL-8490, Chalk River Nuclear Laboratory, 1984.
33 A. J. C. Wilson, *International Tables of Crystallography Vol. C*, Kluwer Academic Publishers, Dordrecht, 1992, p. 391.
34 G. Shirane, *Acta Crystallogr.*, 1959, **12**, 282.
35 W. Opechowski and R. Guccione, *Magnetic Symmetry*, in *Magnetism, Band IIA*, ed. G. T. Rado and H. Suhl, Academic Press, New York, 1963, p. 105.
36 Note that the maximum temperature of the neutron diffraction was lower than that of the DSC measurements.
37 The thermodynamic factor Ω is the ratio of the thermodynamic probabilities of the low and high temperature phases and is calculated from the transition entropy, $\Delta S = \Delta H/T_t$, by $\Delta S = RT_t \ln \Omega$ where T_t is the transition temperature.
38 L. Delaey, *Diffusionless Transformations*, in *Materials Science and Technology Vol. 5: Phase Transformations in Materials*, ed. P. Haasen, Verlag Chemie, Weinheim, 1991.